Available online at www.sciencedirect.com
SCIENCE DIRECT®
Journal of Magnetic Resonance 165 (2003) 282–292
JMR Journal of Magnetic Resonance
www.elsevier.com/locate/jmr

^{2}H chemical shift anisotropies from high-field ^{2}H MAS NMR spectroscopy

Anne Hauch, Henrik Bildsøe, Hans J. Jakobsen, and Jørgen Skibsted*

Instrument Centre for Solid-State NMR Spectroscopy, Department of Chemistry, University of Aarhus, DK-8000 Aarhus C, Denmark

Received 3 April 2003; revised 21 August 2003

Communicated by Lucio Frydman

Abstract

^{2}H chemical shift anisotropies (CSAs) have been determined for the first time for polycrystalline samples employing ^{2}H MAS NMR spectroscopy at high magnetic field strength (14.1 T). The ^{2}H CSA is reflected as distinct asymmetries in the manifold of spinning sidebands (ssbs) observed for the two overlapping single-quantum transitions. Least-squares fitting to the manifold of ssbs allows determination of the ^{2}H CSA parameters along with the quadrupole coupling parameters. This is demonstrated for KD_2PO_4, $ND_4D_2PO_4$, $KDSO_4$, $KDCO_3$, α-$(COOD)_2$, α-$(COOD)_2 \cdot 2D_2O$, and boehmite (AlOOD) which exhibit ^{2}H shift anisotropies in the range $13 \leqslant \delta_\sigma \leqslant 27$ ppm. For fixed values of the shift anisotropy and the ^{2}H quadrupole coupling it is shown that the precision of the CSA parameters depends strongly on the asymmetry parameter (η_Q) for the quadrupole coupling tensor, giving the highest precision for $\eta_Q \approx 0$. The ^{2}H CSA parameters (δ_σ and η_σ) are in good agreement with ^{1}H CSA data reported in the literature for the corresponding protonated samples from ^{1}H NMR spectra employing various homonuclear decoupling techniques. The determination of ^{2}H quadrupole coupling parameters and ^{2}H (^{1}H) CSAs from the same ^{2}H MAS NMR experiment may be particularly useful in studies of hydrogen bonding since the ^{2}H quadrupole coupling constant and the CSA appear to characterize bond lengths in a hydrogen bond in a different manner.

1. Introduction

Deuterium NMR spectroscopy in combination with lineshape simulations is a well-established tool for investigating structural and dynamic processes in solids and liquid crystals [1–3]. Most studies have employed static-powder ^{2}H NMR using the quadrupolar spin-echo technique in studies of molecular motions for a range of materials such as polymers, liquid crystals [4,5], amino acids [6–8], and zeolitic systems [9–11], where information about rate constants and the mechanism of the molecular motions are obtained from the powder line shape resulting from the quadrupole coupling interaction. Considering the small chemical shift range for ^{2}H, static-powder ^{2}H NMR first of all provides information about the ^{2}H quadrupole coupling constant which typically falls in the range $C_Q = 100$–270 kHz. Information about the ^{2}H isotropic chemical shift has been obtained from ^{2}H MAS NMR experiments employing rotor-synchronized acquisition [12] or double-quantum excitation [13]. Furthermore, it has been shown that observation of the complete manifold of spinning sidebands from the ($m = \pm 1 \leftrightarrow m = 0$) transitions by ^{2}H MAS NMR [14–17] allows precise determination of the ^{2}H quadrupole coupling parameters (C_Q and η_Q) and the isotropic chemical shift (δ_{iso}). Moreover, this method gives a significant increase in S/N as compared to the static quadrupolar-echo experiment and allows resolution of overlapping powder patterns in cases of multiple ^{2}H sites [15–17].

Although ^{2}H NMR generally requires isotopic enrichment, this technique has become an important supplement to solid-state ^{1}H NMR where structural information primarily is derived from the isotropic chemical shift and the ^{1}H chemical shift anisotropy (CSA). However, for the abundant ^{1}H spins, homonuclear dipolar couplings may hamper a direct determination of ^{1}H CSAs by MAS

* Corresponding author. Fax: +45-86196199.
E-mail address: jskib@chem.au.dk (J. Skibsted).

1090-7807/$ - see front matter © 2003 Elsevier Inc. All rights reserved.
doi:10.1016/j.jmr.2003.09.007

NMR and thus methods for homonuclear multiple-pulse decoupling are required. ^{1}H CSA tensors have been determined from (i) static-powder [18] and single-crystal [19,20] NMR spectra employing multiple-pulse line-narrowing methods, (ii) MAS NMR spectra using combined rotation and multipulse spectroscopy (CRAMPS) [21] or the high-order truncating MSHOT-3 homonuclear decoupling sequence [22,23], and (iii) static-powder ^{1}H–^{2}H dipolar NMR spectroscopy on magnetically ^{1}H diluted samples [24].

^{1}H CSA tensors have mainly been reported in studies of O–H···O hydrogen bondings, where early work indicated relationships between $\delta_{iso}(^1H)$ as well as the magnitude of the ^{1}H CSA tensor (i.e., $\Delta\sigma = |\delta_{zz} - \delta_{xx}|$) and the bond length $r_{O\cdots O}$ for the O–H···O hydrogen bonds [25]. Moreover, in that study it was shown that $\delta_{iso}(^1H)$ and the principal component of the ^{1}H tensor perpendicular to the hydrogen bond (i.e., $\sigma_\perp$) exhibit linear correlations with the ^{2}H quadrupole coupling constants determined for the corresponding O–D···O sites. Linear correlations between $\delta_{iso}(^1H)$ and the $r_{O\cdots O}$ bond length have also been reported for carboxylic acids [26], trihydrogen selenites [27], and for metal phosphates and other minerals [28]. Furthermore, correlations between $\delta_{iso}(^1H)$ as well as $C_Q(^2H)$ and the inverse of the hydrogen bond distance ($r^{-1}_{H\cdots O}$) have been observed for a number of ^{1}H/^{2}H sites in hydrogen bonds [29].

In this work, we demonstrate the determination of ^{2}H CSAs from slow-speed ^{2}H MAS NMR spectra recorded at a high magnetic field (14.1 T) by least-squares optimization to the intensities of the spinning sidebands from the ($m = \pm 1 \leftrightarrow m = 0$) transitions. This is illustrated by a determination of the ^{2}H CSA and quadrupole coupling parameters for KD_2PO_4, $ND_4D_2PO_4$, $KDCO_3$, $KDSO_4$, α-$(COOD)_2$, α-$(COOD)_2 \cdot 2D_2O$, and boehmite (AlOOD). With the exception of boehmite, ^{1}H CSAs have been reported for these compounds and the ^{2}H CSA parameters determined here are in good agreement with the ^{1}H CSA data. Thus, information about ^{2}H quadrupole couplings and ^{2}H (^{1}H) CSAs can simultaneously be obtained from high-field ^{2}H MAS NMR spectra without the use of multiple-pulse schemes for reduction of homonuclear dipolar interactions. To our knowledge, ^{2}H CSAs have been reported for α-$(COOD)_2 \cdot 2D_2O$ [30], $KDCO_3$ [31], α-$Ca(COOD)_2$ [32], α-glycine [33], and for the amide and carboxyl hydrogens of *N*-acetyl-D,L-valine [34] in all cases employing single-crystal ^{2}H NMR spectroscopy.

2. Experimental

Samples of KH_2PO_4, $NH_4H_2PO_4$, $KHCO_3$, $KHSO_4$, and α-$(COOH)_2 \cdot 2H_2O$ of analytical purity grade from commercial sources were used without further purification and the deuterated compounds were obtained by recrystallization from D_2O (99.9%, Aldrich, WI, USA). α-$(COOD)_2$ was prepared by heating the dihydrate α-$(COOD)_2 \cdot 2D_2O$ overnight at 130 °C. Boehmite (Catapal B Alumina) was purchased from Condea Vista (Texas, USA) and AlOOD was obtained by hydrothermal treatment of boehmite with D_2O at 220 °C for 3 days.

The solid-state ^{2}H MAS NMR spectra were recorded at ambient temperature on a Varian INOVA-600 (14.1 T) spectrometer ($\nu_L = 92.1$ MHz for ^{2}H) using a homebuilt CP/MAS probe for 5 mm o.d. rotors. Stable spinning frequencies (±2 Hz) were achieved using the Varian rotor-speed controller which controls the drive-gas pressure for a fixed bearing-gas pressure. All experiments used single-pulse excitation with a pulse width of 1.0 μs for a rf-field strength of $\gamma B_1/2\pi = 50$ kHz and relaxation delays of 1–4 s. The magic angle was adjusted by optimization of the linewidths for the spinning sidebands in the ^{2}H MAS NMR spectrum of KD_2PO_4. At optimum magic-angle setting these spinning sidebands (ssbs) exhibit a linewidth of FWHM = 50 Hz at 14.1 T (0.54 ppm). The symmetry of the intensities of the ssbs in ^{2}H MAS NMR spectra may be affected by rf offsets caused by filters or improper cable lengths either between the probe and the preamplifier or of the λ/4 cable in the duplexer of the preamplifier. The length of either of these cables was adjusted employing a spinning frequency of $\nu_R = 7.0$ kHz for ^{2}H MAS NMR spectra of $Ca(OD)_2$, since this sample exhibits a large ^{2}H quadrupole coupling ($C_Q = 262$ kHz) and a small CSA ($\delta_\sigma(^1H) = 9.3 \pm 1$ ppm [35]), the latter being efficiently averaged for $\nu_R = 7.0$ kHz. Thus, a highly symmetric manifold of ssbs is observed for $Ca(OD)_2$ with the proper choice for the length of both of these cables. The ^{2}H isotropic chemical shifts are reported in ppm relative to TMS, employing chloroform ($\delta_{iso}(CDCl_3) = 7.27$ ppm) as an external reference. Simulations [36,37], least-squares optimizations and error analysis [38] of the experimental spectra were performed using the STARS software package, which has been incorporated into the Varian VNMR software.

The quadrupole coupling and CSA parameters are defined as: $C_Q = eQV_{zz}/h$, $\eta_Q = (V_{yy} - V_{xx})/V_{zz}$, $\delta_\sigma = \delta_{iso} - \delta_{zz}$, $\eta_\sigma = (\delta_{xx} - \delta_{yy})/\delta_\sigma$, and $\delta_{iso} = 1/3(\delta_{xx} + \delta_{yy} + \delta_{zz})$ employing the following definition of the principal tensor elements for the CSA ($\boldsymbol{\delta}$) and electric field gradient ($\boldsymbol{V}$) tensors: $|\lambda_{zz} - 1/3\mathrm{Tr}(\lambda)| \geqslant |\lambda_{xx} - 1/3\mathrm{Tr}(\lambda)| \geqslant |\lambda_{yy} - 1/3\mathrm{Tr}(\lambda)|$, where $\lambda_{ii} = \delta_{ii}$, V_{ii}. The Euler angles (ψ, χ, ξ), describing the orientation of the CSA tensor relative to the quadrupole coupling tensor, correspond to positive rotations about $\delta_{zz}(\psi)$, the new $\delta_{yy}(\chi)$, and the final $\delta_{zz}(\xi)$ axis. These angles are defined in the ranges $0 \leqslant \psi \leqslant \pi$ and $0 \leqslant \chi, \xi \leqslant \pi/2$ [39].

3. Results and discussion

Figs. 1A and 2A illustrate ^{2}H MAS NMR spectra of KD_2PO_4 recorded using the spinning speeds $\nu_R = 3.0$

and 7.0 kHz, respectively. In agreement with the crystal structure reported for KD_2PO_4 [40], both spectra exhibit a single manifold of ssbs, where the individual ssbs have a Gaussian-like lineshape with a linewidth of FWHM $\approx$ 50 Hz. Inspection of the spectral regions for the singularities ("horns") at about ± 40 kHz and for the outer edges (i.e., at ± 50 to ± 90 kHz) in these spectra shows distinct asymmetries for the intensities of the ssbs. These asymmetries demonstrate that the spectra are not influenced only by the ^{2}H quadrupole coupling interaction. Similar spectral features have recently been observed in ^{14}N ($I = 1$) MAS NMR spectra of some tetraalkylammonium halides [41] and are ascribed to the presence of a small CSA. Considering the actual ^{2}H spin system and the fact that the ssbs do not exhibit any characteristic lineshapes originating from the second-order quadrupolar interaction suggest that the manifolds of ^{2}H ssbs observed at 14.1 T can be simulated by consideration of only the first-order average Hamiltonians for the quadrupole coupling and CSA interactions (i.e., $\overline{\tilde{H}}_{\mathrm{Q}}^{(1)}$ and $\overline{\tilde{H}}_{\sigma}^{(1)}$ [37]). This approach has been successfully employed for a number of half-integer spin quadrupolar nuclei [37–39]. Least-squares optimization of simulated to experimental ssb intensities for the spectrum recorded at $\nu_{\mathrm{R}} = 3.0$ kHz results in the ^{2}H quadrupole coupling and CSA parameters listed in Table 1 for KD_2PO_4 and the optimized simulation shown in Fig. 1B. To test the validity of the theoretical approach employed in the simulations, a least-squares optimization was performed, which also included the second-order term of the average Hamiltonian for the quadrupole interaction ($\overline{\tilde{H}}_{\mathrm{Q}}^{(2)}$). This optimization resulted in the same ^{2}H parameters as those listed in Table 1.

The optimizations to the spectrum in Fig. 1A show that the ssb intensities are insensitive to the Euler angles (ψ, χ, ξ) describing the relative orientation of the two tensors. This is partly due to the fact that $\eta_\sigma \approx \eta_{\mathrm{Q}} \approx 0$ (Table 1), which implies that the simulated ssb manifold

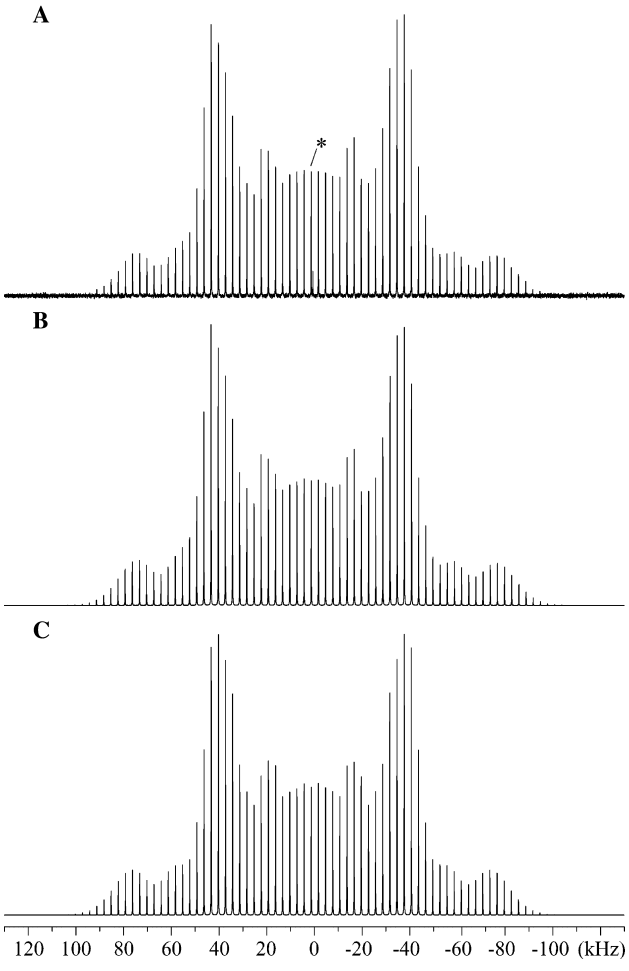

Fig. 1. (A) ^{2}H MAS NMR spectrum (14.1 T) of KD_2PO_4 employing $\nu_{\mathrm{R}} = 3.0$ kHz, a relaxation delay of 1 s, and 2048 scans. The asterisk indicates the isotropic peak. (B) Simulated spectrum employing the optimized ^{2}H quadrupole coupling and CSA parameters listed in Table 1 and assuming coincidence of the two tensors. (C) Simulated spectrum where only the ^{2}H quadrupole coupling interaction has been taken into account and using the C_{Q}, η_{Q}, and δ_{iso} values for KD_2PO_4 in Table 1.

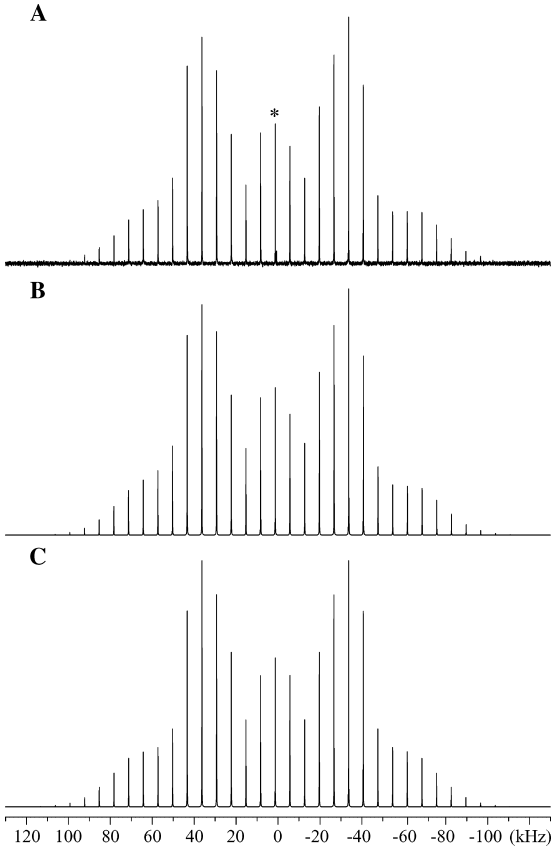

Fig. 2. Experimental (A) and simulated (B and C) ^{2}H MAS NMR spectra (14.1 T) of KD_2PO_4 using $\nu_{\mathrm{R}} = 7.0$ kHz. The simulated spectrum in (B) employs the optimized ^{2}H quadrupole coupling and CSA parameters listed in the text whereas the simulation in (C) only considers the quadrupole coupling interaction. The asterisk indicates the isotropic peak.

Table 1
^{2}H quadrupole couplings (C_Q, η_Q), ^{1}H/^{2}H isotropic chemical shifts (δ_{iso}), and chemical shift anisotropies ($\delta_\sigma, \eta_\sigma$) for the samples studied in this work

Compound	Nucleus	C_Q (kHz)	η_Q	δ_{iso}[a] (ppm)	δ_σ[b] (ppm)	η_σ[b]	Ref.
KD_2PO_4	^{2}H	119.0 ± 0.7	0.06 ± 0.01	13.9	26.7 ± 1.4	0.17 ± 0.16	This work
	^{1}H			14.9	24.9	0.28	[23]
$ND_4D_2PO_4$[c]	^{2}H	119.0 ± 0.6	0.07 ± 0.01	14.8	25.5 ± 1.4	0.09 ± 0.13	This work
$KDSO_4$ Site 1	^{2}H	175.9 ± 0.7	0.14 ± 0.01	11.0	15.4 ± 5.7	0.58 ± 0.23	This work
	^{1}H			12.6	16.2	0.06	[20]
	^{1}H			10.8	16.6 ± 0.2	0.16 ± 0.10	[22]
$KDSO_4$ Site 2	^{2}H	156.4 ± 0.7	0.12 ± 0.01	12.3	17.4 ± 5.3	0.000 ± 0.43	This work
	^{1}H			14.4	18.0	0.09	[20]
	^{1}H			12.1	18.3 ± 0.2	0.45 ± 0.10	[22]
$KDCO_3$	^{2}H	153.1 ± 0.3	0.19 ± 0.01	12.9	18.7 ± 3.0	0.18 ± 0.15	This work
	^{2}H			12.6	17.6 ± 0.3	0.09 ± 0.02	[31]
	^{1}H			16.1	17.8 ± 1.7	0.20 ± 0.12	[20]
AlOOD	^{2}H	212.4 ± 0.7	0.04 ± 0.01	7.4	19.9 ± 2.8	0.09 ± 0.23	This work
α-$(COOD)_2$	^{2}H	177.0 ± 0.5	0.14 ± 0.01	12.9	13.7 ± 2.7	0.43 ± 0.23	This work
	^{1}H			12.6	11.1	0.19	[19,25]
α-$(COOD)_2 \cdot 2D_2O$[d]	^{2}H	116.9 ± 0.2	0.10 ± 0.01	16.4	18.1 ± 1.2	0.48 ± 0.05	This work
	^{2}H			19.8	21.3 ± 2.7	0[e]	[30]
	^{1}H			16.1	19.8 ± 0.2	0.10 ± 0.02	[53]
	^{1}H			18.4	19.8 ± 1.5	0.19 ± 0.06	[54]

[a] The ^{2}H isotropic chemical shifts are corrected for the second-order quadrupolar-induced shift and reported relative to TMS.
[b] The CSA parameters are defined as $\delta_\sigma = \delta_{iso} - \delta_{zz}$ and $\eta_\sigma = (\delta_{xx} - \delta_{yy})/\delta_\sigma$ using the convention $|\delta_{zz} - \delta_{iso}| \geqslant |\delta_{xx} - \delta_{iso}| \geqslant |\delta_{yy} - \delta_{iso}|$.
[c] Parameters for the $D_2PO_4^-$ ion.
[d] Parameters for the ^{2}H ion in oxalic acid.
[e] Axial symmetry ($\eta_\sigma = 0$) was assumed in [30].

is not influenced by the ψ and ξ angles [37]. Moreover, the spectrum is insensitive to variations in the χ angle and thus, this angle cannot be determined from the present spectra. This is a general conclusion for the samples studied in this work and may reflect the fact that ^{2}H MAS NMR spectra are only influenced by small CSAs (i.e., $\delta_\sigma = 10$–25 ppm) and that the unique elements of the electric field gradient (V_{zz}) and CSA (δ_{zz}) tensors are oriented nearly along the internuclear O–H axis, the latter implying that $\chi \approx 0°$. Thus, it is assumed in the simulations that the two tensors coincide. Fig. 1C shows that a simulated spectrum employing the ^{2}H quadrupole coupling parameters for KD_2PO_4, and without taking the CSA interaction into account, results in a symmetric manifold of ssbs around the isotropic peak. Comparison of this spectrum with the simulation in Fig. 1B clearly illustrates the distinct features on the ssb intensities originating from the ^{2}H CSA. Fig. 2 shows that the effects from the ^{2}H CSA are still apparent at higher spinning speeds ($\nu_R = 7.0$ kHz), although somewhat less clear-cut. The simulated spectrum in Fig. 2B corresponds to the result from a least-squares optimization to the experimental ssb intensities in Fig. 2A, resulting in the parameters $C_Q = 118.9 \pm 0.9$ kHz, $\eta_Q = 0.08 \pm 0.04$, $\delta_\sigma = 22.6$ ppm, and $\eta_\sigma = 0.75$ which are in favourable agreement with those (Table 1) determined from the spectrum recorded at lower spinning speed ($\nu_R = 3.0$ kHz, Fig. 1). However, the error analysis for the $\nu_R = 7.0$ kHz spectrum demonstrates that a reliable determination of the CSA parameters cannot be achieved from the spectrum recorded at the higher spinning speed, although the simulations in Figs. 2B and C of this spectrum show that effects from the CSA are clearly observed. Similar analyses of ^{2}H MAS NMR spectra for KD_2PO_4 recorded at $\nu_R = 5.0$ and 4.0 kHz show that the precision of the CSA parameters increases with decreasing spinning speed in agreement with the expectation that highest precision is achieved at the lowest spinning speed. The ^{2}H quadrupole coupling parameters determined from the spectra recorded at $\nu_R = 3.0$ kHz (Table 1) and $\nu_R = 7.0$ kHz are in excellent agreement with those reported earlier for KD_2PO_4 ($C_Q = 119.5$ kHz and $\eta_Q = 0.05$) from a ^{2}H single-crystal NMR study at 30 °C [42]. In addition, the ^{2}H CSA data agree excellently with those determined for ^{1}H in KH_2PO_4 (Table 1) from ^{1}H MAS NMR employing the high-order truncating MSHOT-3 homonuclear decoupling sequence [23].

$ND_4D_2PO_4$ has been studied by ^{2}H MAS NMR using spinning speeds of 3.0 and 8.0 kHz, where the spectrum for $\nu_R = 8.0$ kHz is shown in Fig. 3A. The most intense resonance in the spectrum is the isotropic peak from the ND_4^+ ions, which is flanked by only first- and second-order ssbs at $\nu_R = 8.0$ kHz as a result of motional averaging of the ^{2}H quadrupole coupling for the ND_4^+ ions. The centerband and ssbs for the $ND^+{}_4$

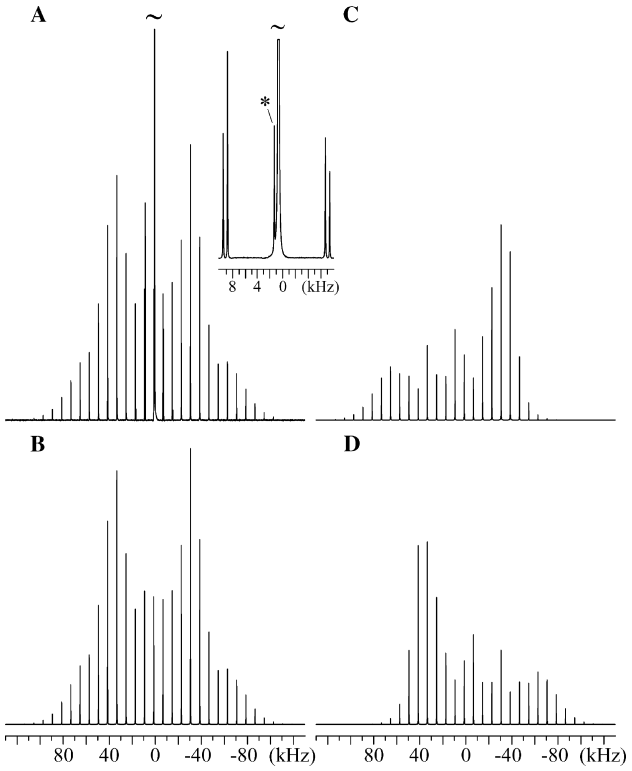

Fig. 3. (A) ^{2}H MAS NMR spectrum of $ND_4D_2PO_4$ ($\nu_R = 8.0$ kHz, 14.1 T) with the centerband from the ND_4^+ ion cut-off at 1/30 of its total height. The inset illustrates the resolution of separate centerbands from the ND_4^+ and $D_2PO_4^-$ (asterisk) ions. (B) Simulated spectrum of the ssbs observed in (A) for the $D_2PO_4^-$ ion, employing the CSA and quadrupole coupling parameters in Table 1. Simulations illustrating the effect of the CSA on the $1 \leftrightarrow 0$ and $0 \leftrightarrow -1$ transitions are shown in (C) and (D), respectively, and correspond to the ^{2}H parameters listed in Table 1 for the $D_2PO_4^-$ ion in $ND_4D_2PO_4$.

ion are completely resolved from the corresponding resonances originating from the $D_2PO_4^-$ ion. Even at a spinning speed of $\nu_R = 8.0$ kHz, distinct asymmetries in the manifold of ssbs are observed for the $D_2PO_4^-$ ion, especially in the spectral region for the "horns" and outer edges. Least-squares optimization to the ssbs from the $D_2PO_4^-$ ion in Fig. 3A gives the parameters $C_Q = 119.2$ kHz, $\eta_Q = 0.07, \delta_\sigma = 25.8$ ppm, and $\eta_\sigma = 0.18$ which correspond to the simulated spectrum in Fig. 3B. An improved precision for these parameters is achieved by optimization to the spectrum recorded at $\nu_R = 3.0$ kHz (not shown) which results in the parameters listed in Table 1 for the $D_2PO_4^-$ ion. The ^{2}H quadrupole coupling parameters are in good agreement with those determined by single-crystal NMR at room temperature ($C_Q = 119.6$ kHz and $\eta_Q = 0.053$) [43] while the ^{2}H CSA parameters are very similar to those determined for KD_2PO_4.

Figs. 3C and D illustrate simulated ^{2}H MAS NMR spectra for the $1 \leftrightarrow 0$ and $0 \leftrightarrow -1$ transitions, respectively, for the $D_2PO_4^-$ ion using the parameters in Table 1. These simulations show that the ^{2}H CSA results in slightly different intensities of the ssbs for the two transitions, especially in the spectral region for the "horns." Furthermore, for one of the transitions, depending on the signs of C_Q and δ_σ, the ^{2}H CSA reduce the spectral width of the transition whereas the width is increased for the other transition. From a theoretical analysis of the corresponding static spectra for the two transitions [42], it is apparent that the difference in width of the two transitions equals $3\delta_\sigma\nu_L$ if axial symmetry and coincidence of the CSA and quadrupole tensors are assumed, i.e., a difference in width of 7.05 kHz for ^{2}H in the $D_2PO_4^-$ ion of $ND_4D_2PO_4$ at 14.1 T. The difference in ssb intensities for the two transitions caused by the CSA strongly depends on the asymmetry parameters η_Q and η_σ, which may affect the precision in the determination of the ^{2}H CSA parameters. The effect of the asymmetry parameters on the precision in the determination of the ^{2}H CSA is investigated in more detail in Fig. 4 which illustrates a contour plot of the *rms* deviation between simulated ssb manifolds for both transitions with and without the consideration of the ^{2}H CSA. The simulations which consider the CSA employ $\nu_R = 3.0$ kHz, $\nu_L = 92.1$ MHz (14.1 T), $C_Q = 120$ kHz and $\delta_\sigma = 25$ ppm (i.e., parameters similar to those observed for the $D_2PO_4^-$ ions in KD_2PO_4 and $ND_4D_2PO_4$, Table 1) and fixed asymmetry parameters in the range $0 \leqslant \eta_Q$, $\eta_\sigma \leqslant 1$. For each set of these parameters the simulated ssb intensities were used as input to a least-squares optimization which disregard the CSA and

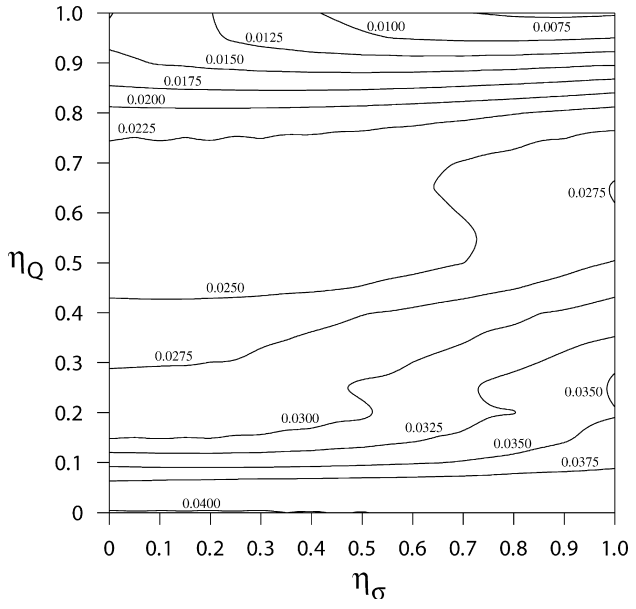

Fig. 4. Contour plot of the *rms* deviation between simulated ^{2}H MAS NMR spectra ($\nu_R = 3.0$ kHz, 14.1 T) in the presence and absence of a CSA ($\delta_\sigma = 25$ ppm) and as a function of the asymmetry parameters η_Q and η_σ. The simulated spectra, which include the CSA, employ a fixed value for the ^{2}H quadrupole coupling constant $C_Q = 120$ kHz whereas the simulated spectra, which do not take the CSA into account, employ optimized values for C_Q and η_Q (see text for further details).

optimize only the quadrupole coupling parameters. Fig. 4 illustrates a contour plot of the *rms* deviation from these optimizations as a function of η_Q and η_σ, where the *rms* deviation is defined as

$$rms = \left\{ \frac{1}{N} \sum_{i=1}^{N} (I^i_{exp} - I^i_{sim})^2 \right\}^{1/2} \quad (1)$$

with I^i_{exp} being the intensity of the simulated ssbs that includes the CSA. These intensities (I^i_{exp}) are normalized relative to the intensity for the most intense ssb in the simulated spectrum. An impression of the effect of the CSA on the ssb intensities is obtained from the *rms* values which give the mean deviation for the ssb intensities relative to the most intense peak. Thus, an increase in *rms* corresponds to a larger deviation between the simulated ssb intensities with and without consideration of the CSA and thereby an improved reflection of the CSA. The contour plot (Fig. 4) shows that the effects of the CSA depend strongly on the η_Q parameter and only to small extent on η_σ. Moreover, it is observed that the best reflection of a CSA of $\delta_\sigma = 25$ ppm is expected for small values of η_Q whereas the combination of large asymmetry parameters for both interactions ($\eta_Q \approx \eta_\sigma \approx 1$) will result in very small effects from the CSA. This may reflect the fact that effects from the CSA are mainly observed for the singularities (''horns''), which are most clearly observed for small η_Q values, and that $\eta_Q \approx 1$ results in very similar effects of the CSA on the two transitions.

The applicability of the method for resolving inequivalent ^{2}H sites is investigated for $KDSO_4$ and $KDCO_3$ by their ^{2}H MAS NMR spectra shown in Figs. 5 and 6, respectively. The ^{2}H MAS NMR spectrum of $KDSO_4$ clearly resolves two manifolds of ssbs, corresponding to very similar quadrupole couplings. Least-squares analysis of these manifolds results in the ^{2}H NMR data listed in Table 1 and illustrated by the simulated spectra in Figs. 5B–D. The observation of two inequivalent ^{2}H sites is in agreement with the single-crystal XRD structure for $KHSO_4$ [44] and an early ^{2}H NQR study which reports the parameters $C_Q = 176.0$ kHz, $\eta_Q = 0.156$ for site 1 and $C_Q = 174.4$ kHz, $\eta_Q = 0.164$ for site 2 [45]. The quadrupole coupling parameters from that work are in good agreement with our data for one of the ^{2}H sites whereas we observe a somewhat smaller C_Q value ($C_Q = 156.4$ kHz) for the other site. Interestingly, this value is in good agreement with the ^{2}H quadrupole coupling ($C_Q = 158$ kHz) predicted in the early work from point-charge calculations [45]. Furthermore, the magnitudes of the ^{2}H CSAs (i.e., δ_σ) determined from Fig. 5 are in good agreement with those reported for the two ^{1}H sites in $KHSO_4$ from ^{1}H single-crystal NMR spectra [20] (Table 1), employing homonuclear decoupling (MREV), and from ^{1}H MAS NMR, using the high-order truncating MSHOT-3 homonuclear decoupling sequence [22] (Table 1). However, a comparison of the η_σ values (Table 1) shows some deviations for the results from ^{2}H and ^{1}H NMR, which suggests that η_σ is less precisely determined from the ^{2}H MAS spectrum of $KHSO_4$ (Fig. 5A) as indicated by the large error limits for this parameter. The resolution of two different ^{2}H sites in the ^{2}H MAS spectrum of $KDSO_4$ is mainly a result of the 1.3 ppm difference in isotropic chemical shifts for the two sites. On the contrary, the ^{2}H MAS NMR spectrum of $KDCO_3$ (Fig. 6A) exhibits only a single manifold of ssbs, where each ssb possesses a quite narrow linewidth (FWHM = 0.7 ppm), although two different ^{2}H sites are reported from a single-crystal neutron diffraction study of

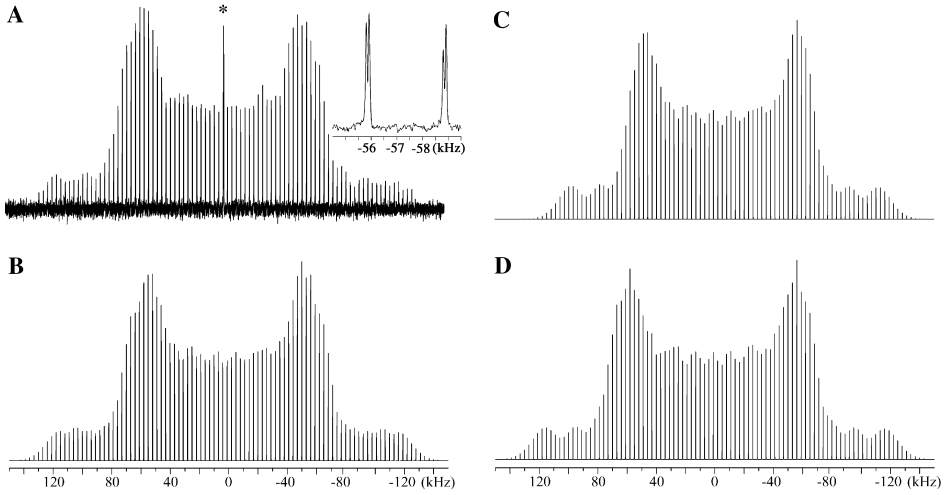

Fig. 5. (A) ^{2}H MAS NMR spectrum of $KDSO_4$ (14.1 T, $\nu_R = 3.0$ kHz). The inset illustrates the resolution of separate ssbs from the two ^{2}H sites in $KDSO_4$ where the individual resonances exhibit widths of FWHM = 0.5 ppm. The asterisk indicates the resonance from a very small amount of mobile D_2O/DOH in the sample. The optimized simulations for the individual ssb manifolds are shown in (D) and (C) for sites 1 and 2 (cf. Table 1), respectively, while a simulation including both sites (from a 1:1 addition of (C) and (D)) is shown in (B). The simulated spectra correspond to the ^{2}H quadrupole couplings and CSAs listed in Table 1 for $KDSO_4$.

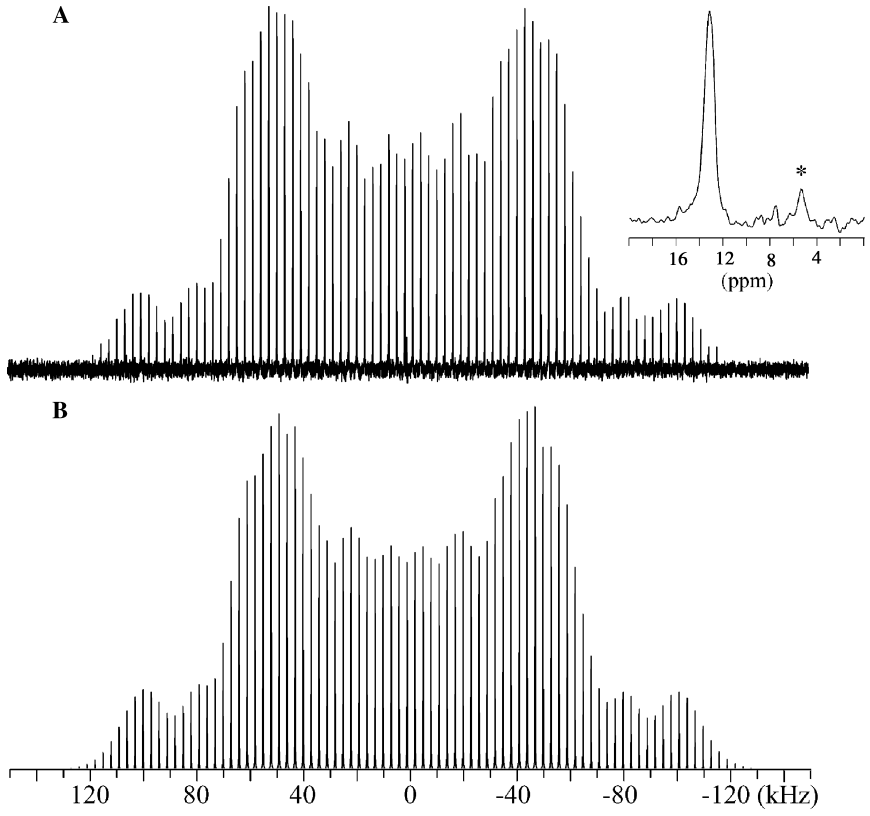

Fig. 6. Experimental (A) and simulated (B) ^{2}H MAS NMR spectra (14.1 T) of $KDCO_3$ employing $\nu_R = 3.0$ kHz. The inset in (A) illustrates the spectral region for the centerbands and the asterisk the centerband from a small amount of mobile D_2O/DOH in the sample. The simulated spectrum corresponds to the ^{2}H NMR parameters listed in Table 1 for $KDCO_3$.

$KDCO_3$ at 298 K [46]. The latter work reports a disordered structure for $KDCO_3$ including two different ^{2}H sites with an estimated relative occupancy of 4:1 which corresponds to the two types of O_2–D$\cdots$$O_3$ and $O_2\cdots$D–O_3 hydrogen bonds in the $(DCO_3)_2^{2-}$ dimer [46]. Poplett and Smith [45] observed separate resonances for the two ^{2}H sites by NQR at room temperature and reported very similar ^{2}H quadrupole coupling parameters for these sites (i.e., $C_Q = 154.7$ kHz, $\eta_Q = 0.189$ for site 1 and $C_Q = 152.6$ kHz, $\eta_Q = 0.193$ for site 2). However, no indication of two different ^{1}H sites in $KHCO_3$ could be inferred from the early ^{1}H single-crystal NMR investigation [20] using homonuclear decoupling (MREV). Thus, ^{1}H CSA parameters have been obtained for an average CSA tensor for the two ^{1}H sites (Table 1). A similar result was obtained in an early ^{2}H single-crystal NMR study of $KDCO_3$ [47], where the quadrupole coupling parameters $C_Q = 154.4$ kHz, $\eta_Q = 0.194$ were reported for a single ^{2}H site. These disagreements between neutron diffraction and ^{1}H/^{2}H NMR have been clarified by Benz et al. [48] from a variable-temperature ^{2}H spin–lattice relaxation study of a single crystal of $KDCO_3$. Their study shows that the hydrogen atoms jump between the two sites and that the exchange rate for this process is fast enough that only an average site is observed by NMR at room temperature. The ^{2}H MAS NMR spectrum in Fig. 6A is quite similar to that reported in an earlier study of $KDCO_3$ [17]. Least-squares optimization to the ssb intensities in Fig. 6A results in the ^{2}H data in Table 1 and in an excellent agreement between the experimental and simulated spectrum (Fig. 6B). Moreover, the ^{2}H NMR data derived from Fig. 6 agree very well with the average quadrupole coupling parameters determined from ^{2}H single-crystal NMR [47] and the average CSA tensor reported from ^{1}H and ^{2}H single-crystal NMR [20,31].

The determination of ^{2}H CSA in the presence of a somewhat larger quadrupole coupling is illustrated in Fig. 7 by the ^{2}H MAS NMR spectrum for a partially deuterated sample of boehmite (AlOO(H,D)). The observation of a single manifold of ssbs is an accord with the crystal structure reported for boehmite from neutron diffraction [49] and least-squares optimization to the experimental ssb intensities results in the ^{2}H parameters listed in Table 1 for boehmite. The larger C_Q value observed for boehmite as compared to the quadrupole couplings for the other compounds studied in this work (Table 1) does not result in a similar increase of the shift anisotropy (δ_σ), indicating that these parameters (C_Q and δ_σ) reflect the hydrogen bonding in a different manner. Sternberg and Brunner [29] have reported a convincing correlation between $C_Q(^2H)$ and the inverse of the hydrogen-bond distance ($r_{H\cdots O}^{-1}$). Employing this

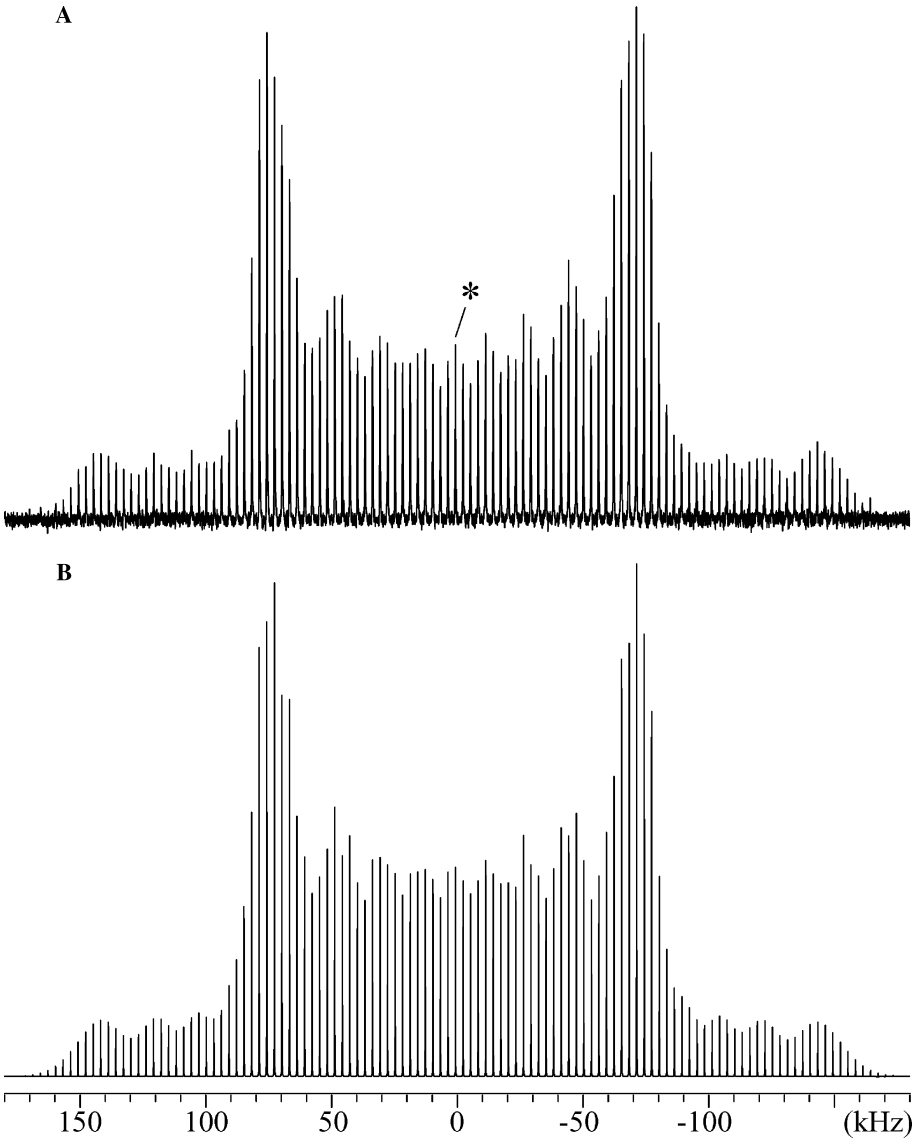

Fig. 7. (A) Experimental ^{2}H MAS NMR spectrum of boehmite (AlOOD) recorded at 14.1 T using a spinning speed $\nu_R = 3.0$ kHz, a relaxation delay of 4 s, and 8192 scans. The asterisk indicates the isotropic peak. (B) Optimized simulation of the spectrum in (A) corresponding to the ^{2}H quadrupole coupling and CSA parameters in Table 1 for boehmite.

correlation and the C_Q value determined for boehmite predicts a hydrogen-bond distance of $r_{H\cdots O} = 1.84$ Å and thereby a hydrogen bond of moderate strength. The predicted value is in very good agreement with the value $r_{H\cdots O} = 1.81 \pm 0.02$ Å reported from powder neutron diffraction for AlOO(H,D) [49], thereby illustrating the potential of ^{2}H MAS NMR in studies of hydrogen bondings in inorganic systems.

Finally, the distinction between ^{2}H in a carboxylic acid and its water of crystallization by ^{2}H MAS NMR is illustrated in Fig. 8 which shows ^{2}H MAS NMR spectra obtained for anhydrous α-$(COOD)_2$ and its dihydrate α-$(COOD)_2 \cdot 2D_2O$. A single manifold of ssbs is observed for α-$(COOD)_2$ (Fig. 8A) in agreement with the reported single-crystal XRD structure [50]. Least-squares fitting to this manifold gives the ^{2}H parameters in Table 1 and the simulated spectrum shown in Fig. 8B. Of the samples studied in this work, the ^{2}H site in α-$(COOD)_2$ exhibits the smallest CSA, which is determined with a decent precision. However, the ^{2}H CSA data are in good agreement with those determined from single-crystal ^{1}H NMR (Table 1), employing the WAHUHA homonuclear decoupling scheme [19]. The ^{2}H MAS NMR spectrum of α-$(COOD)_2 \cdot 2D_2O$ (Fig. 8C) is dominated by a manifold of ssbs with the isotropic resonance at 16.4 ppm and where each ssb exhibits a narrow linewidth (FWHM = 0.76 ppm). This manifold is assigned to the ^{2}H ion of the carboxylic acid, whereas the broad resonances observed in the lower part of the spectrum are ascribed to the water of crystallization. The reduced intensity and significant line broadening of the latter resonances are ascribed to

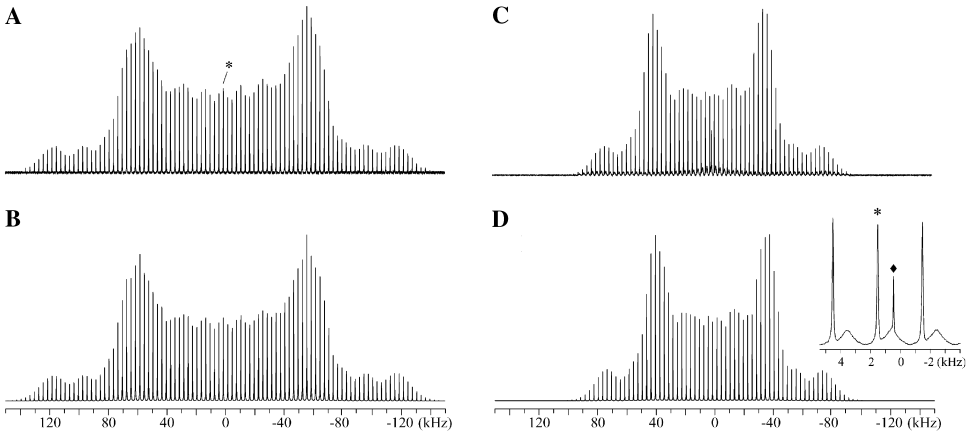

Fig. 8. ^{2}H MAS NMR spectra (14.1 T) of (A) α-$(COOD)_2$ and (C) α-$(COOD)_2 \cdot 2D_2O$ both recorded with a spinning speed of $\nu_R = 3.0$ kHz. The inset in (C) illustrates the narrow ssbs from ^{2}H in oxalic acid and the broad resonances from the mobile crystal water of $(COOD)_2 \cdot 2D_2O$. The asterisks indicate the isotropic peaks and the diamond in (C) a minor resonance from mobile D_2O/DOH in the sample. Optimized simulations of the spectra in (A and C) are shown in (B and D), respectively, and correspond to the ^{2}H data in Table 1 for α-$(COOD)_2$ and α-$(COOD)_2 \cdot 2D_2O$. The resonances from the crystal water in α-$(COOD)_2 \cdot 2D_2O$ have not been included in the simulation in (D).

spectral effects from flipping motions of the water molecules at ambient temperatures, employing the results from theoretical evaluations of molecular motions in ^{2}H MAS NMR [51,52]. The ssbs from the carboxylic acid and the water molecules are fully separated, allowing a straightforward determination of the ^{2}H quadrupole coupling and CSA parameters for the carboxylic acid site from least-squares fitting to the experimental integrated intensities for the ssbs. This gives the ^{2}H data listed in Table 1, where the CSA parameters are in good agreement with those determined earlier from ^{2}H double-quantum NMR of a single crystal [30] as well as with those reported for α-$(COOH)_2 \cdot 2H_2O$ (Table 1) using single-crystal ^{1}H NMR and multiple-pulse homonuclear decoupling [53,54]. A comparison of the ^{2}H parameters with those determined for the anhydrous form of α-oxalic acid shows that the dihydrate exhibits a smaller quadrupole coupling but a larger shift anisotropy (δ_σ) indicating again, that these parameters (C_Q and δ_σ) reflect hydrogen bondings in a different manner.

4. Conclusions

^{2}H chemical shift anisotropies on the order of $\delta_\sigma = 13$–27 ppm can be determined from ^{2}H MAS NMR spectra recorded at a high magnetic field (14.1 T) for a number of polycrystalline solids. The ^{2}H CSA gives rise to distinct asymmetries in the manifolds of spinning sidebands from the two single-quantum transitions, thereby allowing determination of the ^{2}H CSA in addition to the quadrupole coupling parameters by least-squares fitting. However, the ssb intensities in the ^{2}H MAS NMR spectra are found to be insensitive to the Euler angles, describing the relative orientation of the CSA and quadrupole coupling tensors and thus, coincidence of the tensors has been assumed. From a numerical evaluation, the precision of the ^{2}H CSA parameters for a fixed ^{2}H quadrupole coupling constant and a fixed shift anisotropy (δ_σ) is analyzed. The precision is shown to depend strongly on the asymmetry parameter for the quadrupole coupling tensor (η_Q) and results in the highest precision of the CSA parameters for $\eta_Q \approx 0$. The ^{2}H CSA parameters and the isotropic chemical shifts are in good agreement with the corresponding ^{1}H CSA parameters reported for most of the studied samples from ^{1}H single-crystal and MAS NMR experiments employing multiple-pulse homonuclear decoupling sequences. Thus, one of the advantages of the present method is the fact that information about ^{2}H quadrupole couplings and ^{2}H (^{1}H) CSAs can be obtained simultaneously from high-field ^{2}H MAS NMR spectra without the use of multiple-pulse homonuclear decoupling schemes. This approach may be of particular interest in studies of hydrogen bonding in inorganic and organic systems, since it is known from literature that ^{2}H quadrupole coupling constants, ^{1}H (^{2}H) isotropic chemical shifts, and ^{1}H (^{2}H) CSAs are all related, although in a different manner, to the strength of the hydrogen bond.

Acknowledgments

The use of the facilities at the Instrument Centre for Solid-State NMR Spectroscopy, University of Aarhus, sponsored by the Danish Research Councils (SNF and STVF), Teknologistyrelsen, Carlsbergfondet, and Direktør Ib Henriksens Fond is acknowledged. J.S. thanks the Danish Natural Science research Council (J. no. 0001237) for financial support.

References

[1] R.G. Griffin, Solid-state nuclear magnetic resonance of lipid bilayers, in: J.M. Lowenstein (Ed.), Methods in Enzymology, vol. 72, Academic Press, San Diego, 1981, pp. 108–174.

[2] H.W. Spiess, Molecular-dynamics of solid polymers as revealed by deuteron NMR, Colloid Polym. Sci. 261 (1983) 193–209.

[3] G.L. Hoatson, R.L. Vold, ^{2}H-NMR spectroscopy of solids and liquid crystals, in: P. Diehl, E. Fluck, H. Günther, R. Kosfeld, J. Seelig (Eds.), NMR Basic Principles and Progress, vol. 32, Spinger, Berlin, 1994, pp. 1–67.

[4] H.W. Spiess, Structure and dynamics of solid polymers from 2D- and 3D-NMR, Chem. Rev. 91 (1991) 1321–1338.

[5] K. Schmidt-Rohr, H.W. Spiess, Multidimensional Solid-state NMR and Polymers, Academic Press, London, 1994.

[6] L.S. Batchelder, C.H. Niu, D.A. Torcia, Methyl reorientation in polycrystalline amino acids and peptides: a ^{2}H NMR spin–lattice relaxation study, J. Am. Chem. Soc. 105 (1983) 2228–2231.

[7] Y. Hiyama, J.V. Silverton, D.A. Torchia, J.T. Gerig, S.J. Hammond, Molecular structure and dynamics of crystalline *p*-flouro-D,L-phenylalanine. A combined X-ray/NMR investigation, J. Am. Chem. Soc. 108 (1986) 2715–2723.

[8] Y. Hiyama, S. Roy, K. Guo, L.G. Butler, D.A. Torchia, Unusual asymmetry of methyl ^{2}H EFG in thymine: a solid state deuterium NMR and ab initio MO study, J. Am. Chem. Soc. 109 (1987) 2525–2526.

[9] A.J. Vega, Z. Luz, Characterization of NH_4-rho and vacuum-calcined H-rho zeolites by multinuclear NMR spectroscopy, J. Phys. Chem. 91 (1987) 365–373.

[10] D. Goldfarb, H.X. Li, M.E. Davis, Dynamics of water molecules in VPI-5 and $AlPO_4$-5 studied by ^{2}H NMR spectroscopy, J. Am. Chem. Soc. 114 (1992) 3690–3697.

[11] J.M. Kobe, T.J. Gluszak, J.A. Dumesic, T.W. Root, Deuterium NMR characterization of Brønsted acid sites and silanol species in zeolites, J. Phys. Chem. 99 (1995) 5485–5491.

[12] J.L. Ackerman, R. Eckman, A. Pines, Experimental results on deuterium NMR in solid state by magic angle sample spinning, Chem. Phys. 42 (1979) 423–428.

[13] R. Eckman, L. Müller, A. Pines, Deuterium double-quantum NMR with magic angle spinning, Chem. Phys. Lett. 74 (1980) 376–378.

[14] N.J. Clayden, Computer simulations of ^{2}H MAS NMR sideband spectra, Chem. Phys. Lett. 131 (1986) 517–521.

[15] J.H. Kristensen, H. Bildsøe, H.J. Jakobsen, N.C. Nielsen, Deuterium quadrupole couplings from least-squares computer simulations of ^{2}H MAS NMR spectra, J. Magn. Reson. 92 (1991) 443–453.

[16] R.J. Schadt, R.Y. Dong, E. Günther, B. Blümich, Deuteron rotational-echo spectra, J. Magn. Reson. 96 (1992) 393–397.

[17] A.J. Kim, L.G. Butler, Resolving two inequivalent sites with deuterium MAS NMR, J. Magn. Reson. 99 (1992) 292–300.

[18] W.-K. Rhim, D.D. Elleman, R.W. Vaughan, Analysis of multiple pulse NMR in solids, J. Chem. Phys. 59 (1973) 3740–3749.

[19] P.V. Hecke, J.C. Weaver, B.L. Neff, J.S. Waugh, Determination of the proton chemical shielding tensor in anhydrous α-oxalic acid by multiple pulse NMR, J. Chem. Phys. 60 (1974) 1668–1670.

[20] H. Feucht, U. Haeberlen, M. Pollak-Stachura, H.W. Spiess, Multiple pulse proton magnetic resonance study of $KHCO_3$ and $KHSO_4$, Z. Naturforsch. a 31 (1976) 1173–1180.

[21] R.E. Taylor, R.G. Pembleton, L.M. Ryan, B.C. Gerstein, Combined multiple pulse NMR and sample spinning: recovery of ^{1}H chemical shift tensors, J. Chem. Phys. 71 (1979) 4541–4545.

[22] M. Hohwy, J.T. Rasmussen, P.V. Bower, H.J. Jakobsen, N.C. Nielsen, ^{1}H chemical shielding anisotropies from polycrystalline powders using MSHOT-3 based CRAMPS, J. Magn. Reson. 133 (1998) 374–378.

[23] J.T. Rasmussen, M. Hohwy, H.J. Jakobsen, N.C. Nielsen, Magnitude and absolute orientation of ^{1}H chemical shielding tensors in polycrystalline powders: a ^{1}H CRAMPS NMR study of KH_2PO_4, Chem. Phys. Lett. 314 (1999) 239–245.

[24] G. Wu, C.J. Freure, E. Verdurand, Proton chemical shift tensors and hydrogen bond geometry: a ^{1}H–^{2}H dipolar NMR study of the water molecule in crystalline hydrates, J. Am. Chem. Soc. 120 (1998) 13187–13193.

[25] B. Berglund, R.W. Vaughan, Correlations between proton chemical shift tensors, deuterium quadrupole couplings, and bond distances for hydrogen bonds in solids, J. Chem. Phys. 73 (1980) 2037–2043.

[26] R.K. Harris, P. Jackson, L.H. Merwin, B.J. Say, G. Hägele, Perspectives in high-resolution solid-state nuclear magnetic resonance, with emphasis on combined rotation and multiple-pulse spectroscopy, J. Chem. Soc., Faraday Trans. 1 (84) (1988) 3649–3672.

[27] H. Rosenberger, G. Scheler, Y.N. Moskvich, Investigation of hydrogen-bonded compounds using high-resolution NMR spectroscopy in solids, Magn. Reson. Chem. 27 (1989) 50–56.

[28] J.P. Yesinowski, H. Eckert, Hydrogen environments in calcium phosphates: ^{1}H MAS NMR at high spinning speeds, J. Am. Chem. Soc. 109 (1987) 6274–6282.

[29] U. Sternberg, E. Brunner, The influence of short-range geometry on the chemical shift of protons in hydrogen bonds, J. Magn. Reson. A 108 (1994) 142–150.

[30] S. Vega, T.W. Shattuck, A. Pines, Fourier-transform double-quantum NMR in solids, Phys. Rev. Lett. 37 (1976) 43–46.

[31] A.M. Achlama, The chemical shift, dipolar, and quadrupolar tensors of deuterium in potassium bicarbonate, J. Chem. Phys. 74 (1981) 3623–3625.

[32] H. Schmitt, H. Zimmermann, O. Körner, M. Stumber, C. Meinel, U. Haeberlen, Precision measurement of the quadrupole coupling and chemical shift tensors of the deuterons in α-calcium formate, J. Magn. Reson. 151 (2001) 65–77.

[33] C. Müller, W. Schajor, H. Zimmermann, U. Haeberlen, Deuteron chemical shift and EFG tensors in α-glycine, J. Magn. Reson. 56 (1984) 235–246.

[34] R. Gerald II, T. Bernhard, U. Haeberlen, J. Rendell, S. Opella, Chemical shift and electric field gradient tensors for the amide and carboxyl hydrogens in the model peptide *N*-acetyl-D,L-valine. Single-crystal deuterium NMR study, J. Am. Chem. Soc. 115 (1993) 777–782.

[35] L.B. Schreiber, R.W. Vaughan, The chemical shift tensor for the hydroxyl proton: $Ca(OH)_2$, Chem. Phys. Lett. 28 (1974) 586–587.

[36] J. Skibsted, N.C. Nielsen, H. Bildsøe, H.J. Jakobsen, Satellite transitions in MAS NMR spectra of quadrupolar nuclei, J. Magn. Reson. 95 (1991) 88–117.

[37] J. Skibsted, N.C. Nielsen, H. Bildsøe, H.J. Jakobsen, ^{51}V MAS NMR spectroscopy: determination of quadrupole and anisotropic shielding tensors, including the relative orientation of their principal-axis systems, Chem. Phys. Lett. 188 (1992) 405–412.

[38] J. Skibsted, T. Vosegaard, H. Bildsøe, H.J. Jakobsen, ^{133}Cs chemical shielding anisotropies and quadrupole couplings from magic-angle spinning NMR of cesium salts, J. Phys. Chem. 100 (1996) 14872–14881.

[39] J. Skibsted, N.C. Nielsen, H. Bildsøe, H.J. Jakobsen, Magnitudes and relative orientation of ^{51}V quadrupole coupling and anisotropic shielding tensors in metavanadates and KV_3O_8 from ^{51}V MAS NMR Spectra. ^{23}Na quadrupole coupling parameters for α- and β-$NaVO_3$, J. Am. Chem. Soc. 115 (1993) 7351–7362.

[40] W.H. Baur, Reconstruction of local atomic environments in the disordered hydrogen-bonded crystal structures of paraelectric ammonium dihydrogen phosphate and potassium dihydrogen phosphate, Acta Crystallogr. B 29 (1973) 2726–2731.

[41] T. Giavani, K. Johannsen, C.J.H. Jacobsen, N. Blom, H. Bildsøe, J. Skibsted, H.J. Jakobsen, Unusual observation of nitrogen chemical shift anisotropies in tetraalkylammonium halides by ^{14}N

MAS NMR spectroscopy, Solid State Nucl. Magn. Reson. (2003) (in press).
[42] J.L. Bjorkstam, Deuteron nuclear-magnetic-resonance study of the ferroelectric phase transition in deuterated triglycerine and KD_2PO_4, Phys. Rev. 153 (1967) 599–605.
[43] R. Blinc, J. Slak, I. Zupani, Deuteron magnetic resonance study of the antiferroelectric phase of $ND_4D_2PO_4$, J. Chem. Phys. 61 (1974) 988–991.
[44] F.A. Cotton, B.A. Frenz, D.L. Hunter, The structure of potassium hydrogen sulfate, Acta Crystallogr. B 31 (1975) 302–304.
[45] I.J.F. Poplett, J.A.S. Smith, Deuteron quadrupole resonance studies. Part 8.—$^1H/^2H$ double resonance in some inorganic hydroxy compounds, J. Chem. Soc., Faraday Trans. 2 74 (1978) 1077–1087.
[46] J.O. Thomas, R. Tellgren, I. Olovsson, Hydrogen bond studies. XCII: disorder in $(HCO_3)_2^{2-}$ and $(DCO_3)_2^{2-}$ dimers: a neutron diffraction study of $KHCO_3$ and $KDCO_3$, Acta Crystallogr. B 30 (1974) 2540–2549.
[47] T. Chiba, Deuteron magnetic resonance study of some crystals containing an O–D···O bond, J. Chem. Phys. 41 (1964) 1352–1358.
[48] S. Benz, U. Haeberlen, J. Tegenfeldt, Jump motion of deuterons along hydrogen bonds in $KDCO_3$. A deuteron relaxation study, J. Magn. Reson. 66 (1986) 125–134.
[49] A.N. Christensen, M.S. Lehmann, P. Convert, Deuteration of crystalline hydroxides. Hydrogen bonds of γ-AlOO(H,D) and γ-FeOO(H,D), Acta Chem. Scand. A 36 (1982) 303–308.
[50] J.L. Derissen, P.H. Smit, Refinement of the crystal structures of anhydrous α- and β-oxalic acids, Acta Crystallogr. B 30 (1974) 2240–2242.
[51] J.H. Kristensen, H. Bildsøe, H.J. Jakobsen, N.C. Nielsen, Theory and simulations of molecular dynamics in ^2H MAS NMR, J. Magn. Reson. 100 (1992) 437–443.
[52] O. Weintraub, S. Vega, Dynamic ^2H nuclear magnetic resonance of rotating solids, Solid State Nucl. Magn. Reson. 4 (1995) 341–351.
[53] S. Sagnowski, S. Aravamudhan, U. Haeberlen, Proton magnetic shielding in crystals of α-oxalic acid dihydrate. Comparison with deuteron shielding, J. Chem. Phys. 66 (1977) 4697–4698.
[54] B. Berglund, R.W. Vaughan, A multiple pulse proton NMR study of α-oxalic acid dihydrate, J. Chem. Phys. 72 (1980) 3424–3426.